Near infrared low coherence speckle interferometry (NIR-LCSI) as a tool for the investigation of silicon in solar cell production

Kay Gastinger[1] and Lars Johnsen
SINTEF ICT, Trondheim, Norway

ABSTRACT

A setup for an NIR-LCSI instrument is introduced. It is based on a Superluminescence diode (SLD) (wavelength = 1280nm, FWHM = 50nm) and an InGaAs camera with VGA resolution. The paper presents a work in progress. The aim of the research work is to measure the chipping process in a Si wafer saw with high spatial resolution. Hereby the sawing channel inside the silicon block is investigated. The chipping generates a change of the interface topography of the sawing channel. NIR-LCSI will be applied to measure this topography change and contributes thus to determine the size and volume of the silicon chips and thus the cutting rate of the sawing process. This paper presents a novel concept to increase the spatial resolution of the imaging system. With the use of a new type of "immersion" optics the numerical aperture can be significantly increased and a spatial resolution close to, or even below, the nominal illumination wavelength can be obtained. The speckle size and the resulting spatial and depth resolution of the LCSI measurements are investigated.

Keywords: Low Coherence Speckle Interferometry (LCSI), Near Infrared (NIR) Interferometry, Optical Coherence Tomography (OCT), Electronic Speckle Pattern Interferometry (ESPI), Low Coherence Interferometry (LCI), Optical Coherence Microscopy, Solar Cell Inspection, Tribology

1. INTRODUCTION

Low Coherence Speckle Interferometry (LCSI) [1] is a relatively new technique within speckle metrology. It combines two techniques; Optical Coherence Tomography (OCT) and traditional Electronic Speckle Pattern Interferometry (ESPI). OCT provides the ability to measure depth resolved structures inside a material. ESPI measures the deformation pattern of an object with high accuracy. Consequently, LCSI provides a versatile tool for the depth resolved measurement of deformations inside an object.

Moving LCSI toward the Near InfraRed (NIR) opens the opportunity to investigate the internal structure of materials not transparent in the visible wavelength range. The extensive use of Silicon (Si) in micro- and nano fabrication and in particular in the solar cell industry puts a research focus on this material. Low doped Si is almost transparent in the NIR region for wavelength larger then 1250nm.

The major part of the solar cell production is today based on silicon wafers. The wafers are produced in a multi wire saw, where the silicon blocks are cut into about 180µm thick wafers. The sawing process is based on a sawing fluid (slurry) consisting of Polyethylene Glycol (PEG) as a carrier and Silicon Carbide (SiC) as cutting particles. Figure 1 shows the principle configuration of a multi wire saw and its main components.

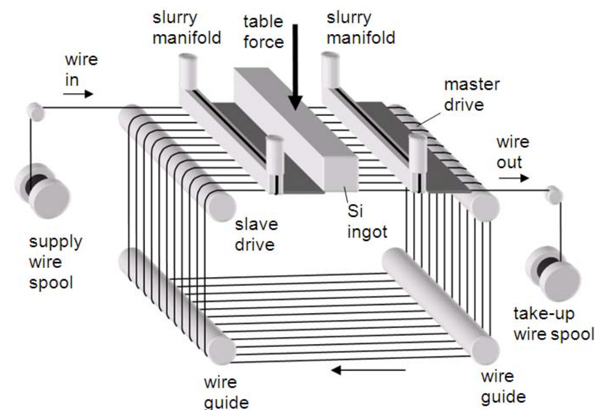

Figure 1 Multi- wire saw for Si-wafer production

Si wafer sawing is a tribological process where wear (due to the abrasive SiC particles), lubrication (by polyethylene glycol - PEG) and friction (caused by contact between the wire, the abrasive SiC particles and the Si ingot) play important roles (figure 2). However the sawing is not yet fully understood. A widely accepted theory is that the SIC particles introduce micro cracks in the Si material. These cracks propagate and small silicon chips are removed. To reduce the wafer thickness further and to optimise the wafer quality a better understanding of this abrasive process is required.

[1] kay.gastinger@sintef.no

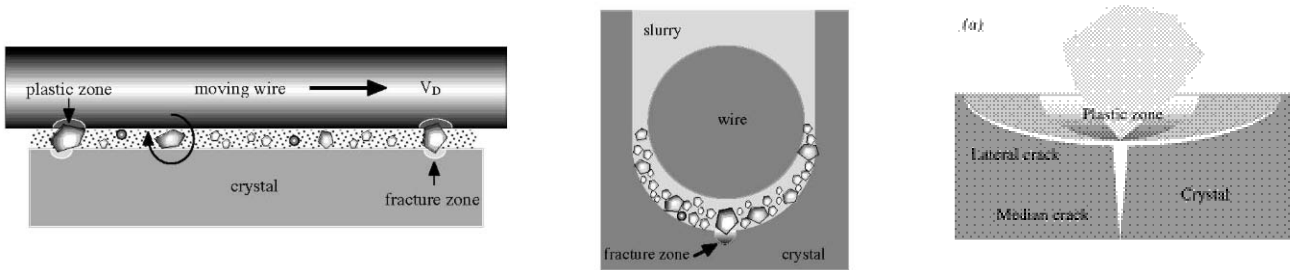

Figure 2 Illustration of the cutting process, left: cross section perpendicular to the wire direction, centre: cross section in wire direction, right: model of the indent of a single particle (courtesy [1,2])

Different attempts have been made to model the actual material removal in the silicon cutting process. However, in-situ measurements of the contact during cutting in order to reveal acting processes are still a challenge. In-situ measurements would represent a good basis for simulating the cutting process, since the plastic deformation of the materials in contact, chipping and micro-chipping, the distribution of PEG and SiC particles and the wear processes could be studied in real time.

The presented work aims to develop a novel setup for in-situ, high accuracy investigation of the contact area in a simulated cutting process at lab scale. In particular the investigation of the chipping process is of interest.

2. LOW COHERENCE SPECKLE INTERFEROMETRY IN THE NEAR INFRA RED (NIR)

Optical profilers, based on microscopic low coherence interferomtery, are widely used for the high accuracy inspection of the topography of surfaces. With diffraction limited resolution in the lateral dimensions and nanometer to sub-nanometer resolution in the longitudinal direction this techniques are well suited for many industrial applications. LCI is also referred to as white-light interferometry

Optical Coherence Tomography (OCT) systems [3], in particular used for medical applications, have been developed. These systems enable the measurement of the inner structure of an object. The first OCT systems for material inspection are recently approaching the marked [4]. The depth resolution of these systems is in the range of 1-50µm and defined by the FWHM of the interference envelope in a Michelson interferometer. The basic configuration of a low coherent Michelson interferometer can be seen in figure 3. The technique utilises the temporal coherence of a broad band light source for high accuracy mapping of the inner structure in a material.

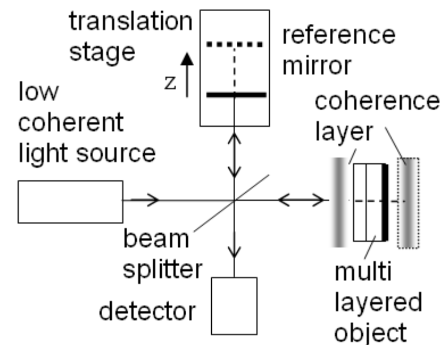

Figure 3 Michelson type low coherence interferometer

On the other hand Electronic Speckle Pattern Interferometry (ESPI)[5] is a well-established technique for high accuracy deformation measurements of objects with rough surfaces.

Combining the functionality of these interferometric techniques enables the high resolution, depth resolved measurement of changes at interfaces inside a material. This has been introduced as Low Coherence Speckle Interferomtery (LCSI) [6]. The measurements start with a scan of the reference mirror. Thus the inner structure of the object is mapped. Then the interface to be investigated is identified and aligned at the position of maximum contrast of the coherence layer. Finally, the investigation of changes at this interface can be carried out using the deformation measurement algorithms of ESPI based on interferometric phase measurements.

In the here presented paper LCSI is applied in the NIR for the inspection of silicon material. The main challenges are the long wavelength, limiting the spatial resolution of the imaging system, and the high refractive index of the silicon. Furthermore, standard CCD cameras are not sensitive in this wavelength region. The paper presents work in progress. It addresses the challenges of the described application and gives a first proof of principle for NIR LCSI.

3. OPTICAL CONFIGURATION

NIR-LCSI can contribute to investigate the sawing process in-situ. However applying LCSI for Si creates some challenges. One main challenge addressed in this paper is to achieve high enough spatial resolution to study the abrasive process.

3.1. Imaging system

3.1.1. Spatial resolution

The features to be detected (silicon chips) are in the range of 5-10µm in lateral dimensions. This requires high lateral resolution. The resolution of the imaging system in LSCI can be limited by the spatial resolution of the optical system and the speckle size.

Optical resolution

For high resolution imaging it is necessary to use short wavelength illumination and optics with high numerical aperture (NA). An often used expression for the spatial resolution Δx is [7]:

$$\Delta x = \frac{4\lambda_c}{\pi} \frac{1}{2NA} \tag{1}$$

where λ_c is the centre wavelength and NA denotes the numerical aperture of the imaging system.

The absorption properties of silicon require the use of light with a relative long wavelength in the NIR range (wavelength > 1250nm). Therefore the wavelength of the low coherent light source is selected close to this limit (λ_c=1280nm in air). However this is still about a factor 2-3 larger than in conventional microscopy.

To increase the spatial resolution the numerical aperture of the imaging system can be increased. However, in particular the high refractive index of n_{Si}=3.51 (for λ=1280nm) limits the achievable effective NA and thus the spatial resolution of the imaging system. This can be seen in figure 4. Light reflected with an angle larger than 16.55° from normal incident is total reflected and does not contribute to imaging. An imaging system using a microscope objective with an NA of 0.4 will only detect light within an angle of 6.54°. The effective NA inside the silicon is thus limited to NA_{Si}=0.11. On the other hand the wavelength of the light inside the silicon is given by

$$\lambda_{c,Si} = \frac{\lambda_{c,air}}{n_{Si}} \tag{2}$$

Thus the spatial resolution inside the silicon is given by

$$\Delta x_{Si} = \frac{4\lambda_{c,air}}{n_{Si}\pi} \frac{1}{2NA_{Si}} \tag{3}$$

Both resolutions are thus about the same: $\Delta x_{Si} \approx \Delta x_{air}$ = 2,1µm.

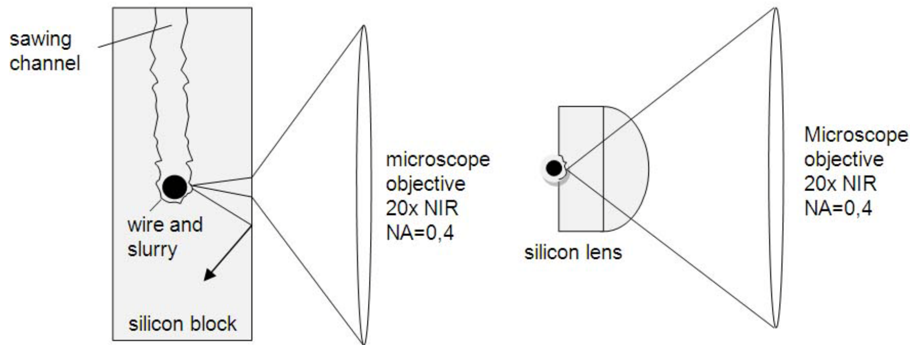

Figure 4 Optimising the numerical aperture of the imaging system, left: saw channel with standard imaging configuration, right: sawing process in a silicon lens to increase the NA of the imaging system.

In order to increase the spatial resolution in the given application only an increasing of the NA can contribute. Therefore the configuration shown in the right sketch in figure 4 is suggested. Usually an index matching liquid eliminating the air interface between the object and the first lens of the optical system is used to improve the lateral resolution. However for the high refractive index of Si no suitable index matching liquid is available. To overcome this, the silicon surface can be adapted to the path of the optical rays in the system. This can be achieved by introducing a custom made spherical Si-lens as the sample under test and investigating the sawing process close to the centre of curvature of the lens. Thus the optical rays are only slightly refracted at the Si surface and we can increase the effective NA of the system close to the NA of the microscope objective. In the suggested design we use a single convex Si-lens with radius of curvature of 8mm and 8mm centre thickness.

	Surf:Type	Radius	Thickness	Glass	Semi-Diameter	Conic	Par 1(unused)
OBJ	Standard	Infinity	8.000000	SILICON	5.000000E-003	0.000000	
STO*	Standard	-8.000000	12.000000 V		6.250000 U	0.000000	
2	Paraxial		12.000000		7.334636		10.000000
3	Paraxial		160.000000		2.944351		-8.421053
IMA	Standard	Infinity	-		0.349901	0.000000	

Figure 5 Zemax model of a similar system using ideal lenses for the 20x Mitutoyo objective since the optical design of the objective is not known.

A similar optical system is modelled in Zemax (figure 5). The obtained magnification of such a system is 70x. Using the suggested optical design a diffraction limited spatial resolution of $\Delta x \approx 0,6\mu m$ can be obtained. In a real system the spatial resolution is limited by aberrations and the expected resolution is about $\Delta x \approx 1\mu m$.

Speckle size

The speckle size limits the spatial resolution of ESPI systems. For microscopic ESPI this issue has been discussed by Løkberg et al. [9] and El-Jarad [10]. The medium speckle size at the detector d_s can be calculated from [10]

$$d_s = 1{,}22\lambda_c \frac{M}{2NA} \tag{4}$$

where M is the magnification of the system. The resolution of the speckle pattern at the object d_o can be calculated from the d_s [10]. However we need to consider that the object is inside the silicon material. Therefore the modified equation can be given by:

$$d_o = \frac{d_s}{n_{Si} M} = 1{,}22 \frac{\lambda_c}{n_{Si}} \frac{1}{2NA} \tag{5}$$

Using the parameters of our imaging system the typical speckle size of d_o=0.55µm. Due to the large variation of the speckle size by the speckle pattern and the introduced disturbances due to low speckle modulation, d_o is not corresponding to the lateral resolution of the system. Løkberg et al. assumes an area of about 5x5 speckles is necessary to detect a deformation.

In the given LCSI system the calculation of the object speckle size is not straight forward. The speckle size at the detector can be calculated from (4). However if we want to calculate the resolution in the object space the high refractive index of Si needs to be considered. This issue is currently investigated and will be an object of further research.

3.1.2. Depth resolution

The depth resolution of a full-field OCT system is determined by the depth of focus of the imaging system and by the coherence length of the light source [7].

Temporal coherence of the source

For imaging systems with a low NA the temporal coherence of the light source determines the depth resolution. The equation commonly used for the depth resolution in an interferometer is given by [7]

$$\Delta z_{c,air} \approx \frac{2ln2}{\pi}\left(\frac{\lambda_{c,air}^2}{\Delta\lambda}\right) \tag{6}$$

where $\Delta\lambda$ is the FWHM of the light source. Solving this equation with the given parameters results in a depth resolution of about $\Delta z_{c,air}$=14.5 µm. Since both $\lambda$and $\Delta\lambda$ are scaled by the wavelength the corresponding coherence length in Si is

$$\Delta z_{c,Si} \approx \frac{2ln2}{n_{Si}\pi}\left(\frac{\lambda_{c,air}^2}{\Delta\lambda}\right) \tag{7}$$

This results in $\Delta z_{c,Si}$ =4.1µm which is often defined as the depth resolution in silicon for lower NA.

Depth of focus

For imaging systems using a high NA, the depth of focus becomes the limiting factor for the depth resolution [8]

$$\Delta z_{opt,air} = \frac{\lambda}{\pi NA^2} \tag{8}$$

For the parameters in the presented application this results in a $\Delta z_{opt,air}$=2.55 µm for NA=0.4 and $\Delta z_{opt,air}$ =33.7µm for NA=0.11. Again for measurements in silicon the wavelength scales with the refractive index giving

$$\Delta z_{opt,Si} = \frac{\lambda}{n_{Si}\pi NA^2} \tag{9}$$

This results in a $\Delta z_{opt,Si}$ =0.7µm for NA=0.4 and $\Delta z_{opt,Si}$ =9.6µm for NA=0.11. Thus for NA=0.11 and the temporal coherence of the source defines the depth resolution while for NA=0.4 the depth of focus is deciding. In praxis the interference signal can be detected over a larger range as defined in (7) and we can accept defocusing exceeding the Rayleigh criteria given in (8). Thus these parameters should be optimised and verified in the further experimental work.

In OCT the depth resolution should be as high as possible. Thus the numerical aperture in such systems is designed to be large and the coherence length of the light source small. However, in LSCI, applied for the given application, the coherence length should be sufficient long to cover the whole surface depth, but short enough to extract the interferometric information coming from the interface under investigation. Thus the depth of focus should be large enough to image all features of the interface sufficiently. It is given that this is a trade of between the spatial resolution and the depth of field.

3.2. Interferometer system

The interferometer system can be build up in different configurations. Our long term aim is to develop a Mirau configuration since this configuration seems to be most reliable and stable regarding environmental disturbances. However, because of the necessity of dispersion compensation in the low coherence interferometer the design is more sophisticated. Thus, at this stage we introduce a combination of a Michelson and Linnik type of interferometer shown in figure 6.

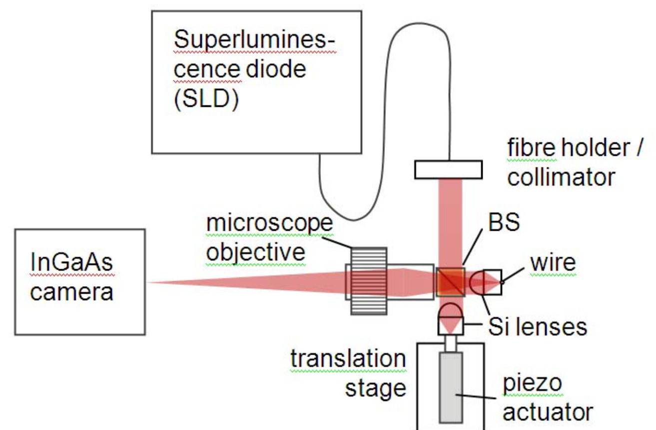

Figure 6 Interferometer configuration for investigating the saw channel

The light from a fibre coupled SLD (Superlum 1300) with a centre wavelength of 1280nm and a FWHM of the near Gaussian wavelength distribution of 50nm is collimated. The optical power of the SLD is up to 20mW. A cube beam splitter divides the incoming beam into a reference and an object beam. The object beam is directed towards the silicon lens and reflected at the saw channel introduced by a steel wire and some slurry.

The reference beam is directed towards an identical lens without saw channel. Using this configuration the reflectivity of the object and reference beam is similar. Furthermore the amount of silicon in both arms is the same when the sawing process is started. This is strongly necessary since the high refractive index leads to an extinction of the interferometer signal due to dispersion. The silicon lens in the reference arm is mounted on a piezo actuator. The actuator again is mounted on a translation stage. The translation stage is used for structural imaging of the object and adjusting the coherence layer at the back surface of the object lens. The piezo enables phase shifting. The reflected beams interfere in the beam splitter and the interference fringes are imaged onto the camera by a microscope objective.

The imaging system consists of a Mitutoyo 20x NIR optimised microscope objective with an NA of 0.4. The working distance of the objective is 2cm and the focal length 1cm. The NIR camera is a Xenics Xeva-1.7-640. The camera has sensitivity in the wavelength range from 0.9µm to 1.7µm and comes in VGA resolution 640x512 pixels. The pixel pitch is 20 µm. The maximum frame rate is 90fps at full resolution. For lower resolutions the frame rate can be increased up to 200fps.

Measurement speed

A critical factor for the in-situ inspection of the sawing process is the measurement speed. The typical wire velocity is about 12m/s. This requires high speed imaging to follow the process on the surface of the sample. The field of view (FoV) of the measurement is about 200x150µm. A fixed point of the wire needs thus about 16µs to move over the FoV. An extreme high frame rate would be necessary to inspect the area within this timeframe. However the chipping rate is uncertain. Further investigations are necessary to investigate the optimum frame rate.

In laboratory conditions we can slow down the process to inspect the microscopic processes. Experiments will show which frame rate is necessary to investigate the real processes. The InGaAs camera is today available with up to 2000fps.

4. EXPERIMENTAL SETUP FOR PROOF OF PRINCIPLE

This chapter presents a first proof of principle for NIR LCSI. Since a work in progress is presented the targeted configuration presented in chapter 3 could not yet be tested. However, we have been able to test all components on the surface of two different silicon samples. The adjustment of the coherence layer at the surface and speckle based deformation measurements are demonstrated.

4.1. Samples

The applied silicon samples are results from the sawing experiment in a single wire saw. One of the samples is polished on the surface the other one has an as cut surface. The size of the samples is about 5cm x 5cm. Both samples are cut about half way and then the sawing is stopped. This gives the possibility to simulate the cutting process in the lab by introducing the wire and slurry in the sawing channel and simulating the sawing movement. Pictures of both samples can be seen in figure 7. The sawing channels are clearly visible.

Sample 1 is polished on the surface to be able to access the sawing area. The surface of the sawing area is rough. In the given experiment a single wire configuration is used.

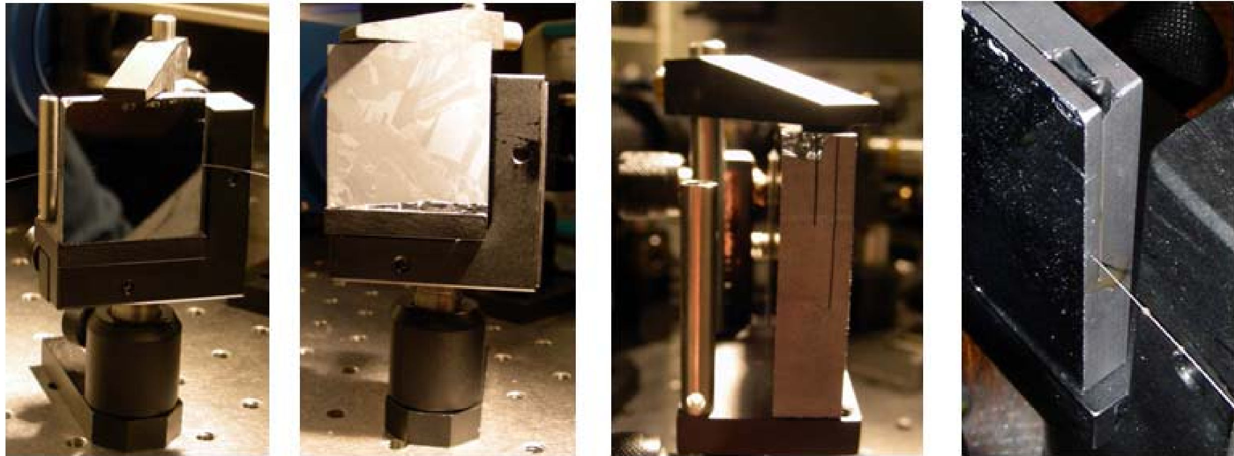

Figure 7 Sample used for proof of principle from left: 1: polished surface, 2: as cut surface, 3: saw channels seen from the side, 4: wire in the saw channel with slurry applied

4.2. Experimental Setup

The optical setup is based on a Michelson interferometer and very close to the final setup presented in chapter 3 (figure 8). The main difference is the microscope objective which here is an OPTEM NIR Zoom 7x objective with a 2x auxiliary lens. The magnification can be adjusted from 1.5x to 10.5x. The working distance is 80mm which gives more space for the interferometer and makes it possible to vary the field of view. The NA is rather small and varies from 0.08 to 0.16 with the magnification.

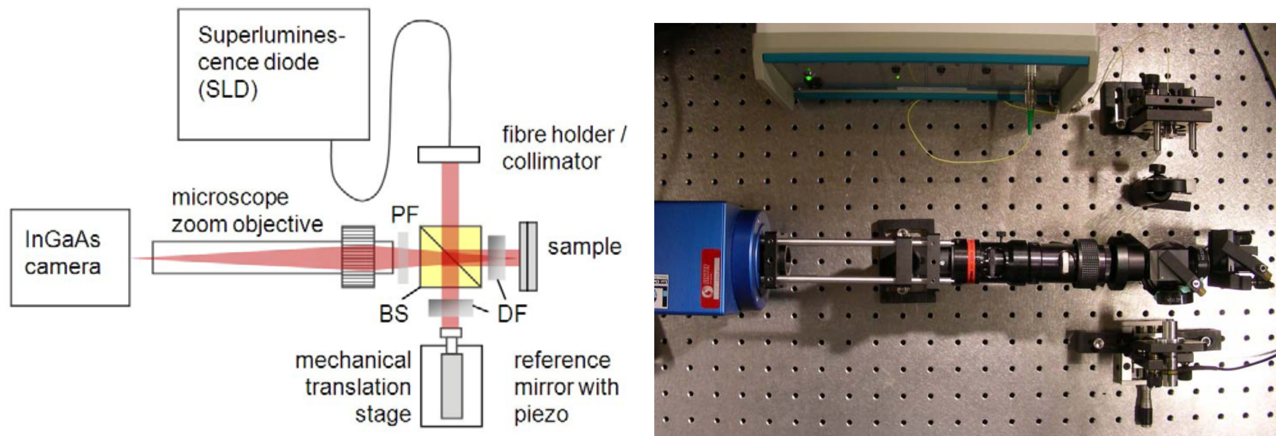

Figure 8 Experimental setup for the proof of concept, left: sketch of the setup, right: photograph

Furthermore the suggested lens configuration of the object in order to increase the NA is not yet implemented. We measure thus on plane silicon samples that results in even lower NA for measurements inside the object. For surface measurement dispersion compensation is not required. However it was necessary to adapt the intensity in object and reference arm with density filters. To avoid dispersion effect density filters with the same thickness are included in both interferometer arms but with different attenuation. Polarisation filters reduce the incoherent background light. This is advantageous in particular for the rough surface measurements. A manual translation stage is included in the reference arm to control the position of the coherence layer.

5. EXPERIMENTAL RESULTS

5.1. Polished surface

The first results from the measurements on the polished sample surface can be seen in figure 9. The left image shows the camera view of the object using back light illumination. The field of view is about 2mm x 2mm. In the centre object the coherence layer is adjusted at the sample surface and the sample surface is adjusted almost perpendicular to the observation direction. A number of fringes occur. The mod-2π phase map of the fringes is detected using a standard temporal phase shifting algorithm

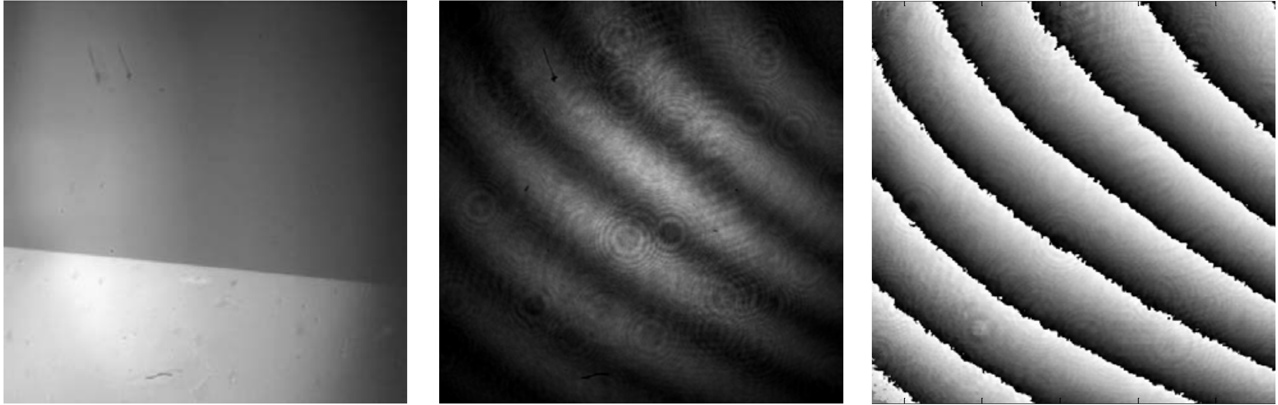

Figure 9 Results the polished sample surface, left: image of the silicon sample with backlight illumination, centre: interference fringes from the polished front surface, right: mod-2π phase map of the interference fringes.

5.2. Rough surface

The measurements on the as-cut surface of the silicon demonstrate the ability of the setup to measure deformations on rough surface. This is important as the sawing channel inside the object has the same surface characteristic as the here applied surface.

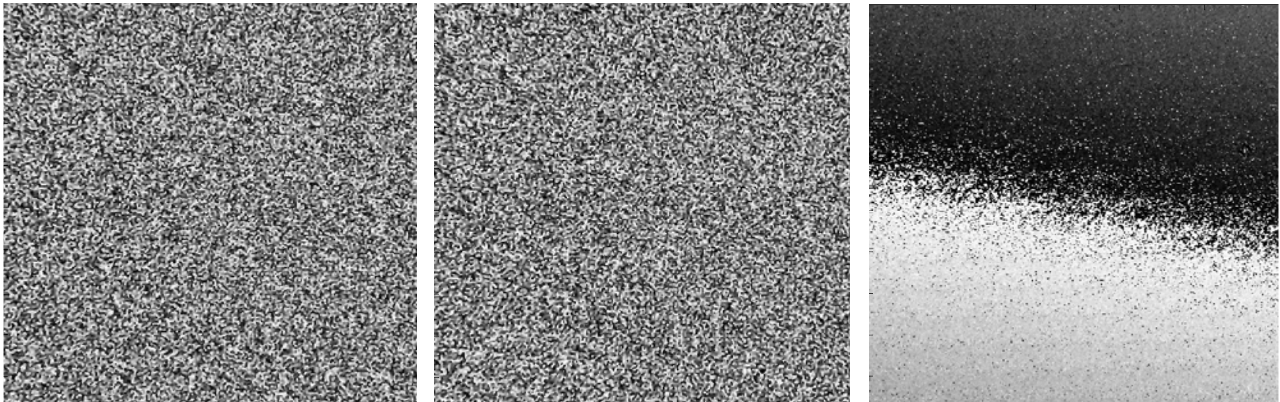

Figure 10 Deformation measurement on the surface of the rough sample, left and centre: mod-2π phase maps, before and after deformation, right: deformation phase map for a slightly tilted object.

Figure 10 shows the well known speckle phase maps and deformation phase maps from ESPI. The only difference is that in LSCI the coherence layer needed to be adjusted at the surface of the sample and the sample was adjusted at the maximum position of the coherence envelope. The two mod-2π phase maps, before and after deformation, are seen in the left and centre image in figure 10. Between the two recordings the object was slightly tilted in vertical direction. The right image in figure 10 shows the difference of the two phase maps corresponding to the deformation of the object (coded in grey levels).

6. CONCLUSIONS AND FUTURE WORK

We present a work in progress. The here presented work demonstrates LCSI in the NIR region for wavelengths larger than 1250nm. Besides the application of a NIR light source it has to be considered that standard silicon based CCD cameras are not sensitive for light in this wavelength range. Therefore a camera based on InGaAs as detector material is applied. The main challenges when applying LCSI at such large wavelengths are to obtain high spatial resolution and maintain at the same time sufficient depth of focus and thickness of the coherence layer to cover the whole surface profile.

A novel method is suggested to increase the spatial resolution of the imaging system used in an NIR LCSI system. The surface of the sample is adapted and included in the optical system to avoid the reduction of the NA of the imaging system caused by the refractive index of silicon. A good trade off between spatial resolution and depth of focus as well as a proper selection of the coherence length of the light source is necessary.

Phase measurements on rough and polished surfaces using NIR LCSI are presented. Also, the application of the standard ESPI algorithms for deformation measurements is demonstrated.

The parameters of the designed imaging system are close to the limit of the requirements of the measurement task. However, there is potential to use the introduced setup for measurements of the chipping process during wire sawing of silicon wafers. Furthermore this technique can also be applied for the detection of impurities and defects in the silicon raw material.

The main challenges applying LCSI for measurements inside the silicon material are the compensation of dispersion and the reduction of the incoherent background in the system. A useful approach for this is a spatial filter. Furthermore the adaptation of the beam ratio between the coherent object light and the reference light is demanding. The influence of the speckle size on the spatial resolution needs to be further investigated and experimentally verified. Furthermore also the influence of the dispersion in silicon needs further theoretical and experimental investigation.

ACKNOWLEDGEMENTS

Several people have contributed to the present work. Karl Henrik Haugholt for the optical modelling using Zemax. Sergio Armado, Ole Johan Løkberg, Arne Røyset and Gudmunn Slettemoen have given input of great value to the theoretical investigations. The authors want to thank these people for their valuable contributions. The work is partly financed by the Norwegian Research Council through the user-driven innovation project "TyWatt".

REFERENCES

[1] H.J. Möller, "Basic Mechanisms and Models of Multi-Wire Sawing", Adv. Eng. Mater., **6** 7, 502–513, 2004
[2] H.J. Möller et al. "Multicrystalline silicon for solar cells". Thin Solid Films, 487 (1-2), 179-187, 2005
[3] J. G. Fujimoto, W. Drexler, U. Morgner, F. Kärtner, and E. Ippen, "Optical Coherence Tomography", Opt. Phot. News, 24, 2000
[4] Heliotis AG, www.heliotis.com
[5] O.J. Løkberg, and G.Å. Slettemoen, "Basic electronic speckle pattern interferometry", Applied Optics and Optical Engineering, J.C. Wyant and R. Shannon, Vol.10, 455-504, Academic Press, New York, 1987
[6] K. Gastinger, Low coherence speckle interferometry (LCSI): when speckle interferometry goes sub-surface, SPIE Vol. 7008 Eighth International Conference on Correlation Optics, Malgorzata Kujawinska; Oleg V. Angelsky, Editors, 70081I, 2007
[7] B.E. Bouma and G.J. Tearney, editors, [Handbook of Optical Coherence Tomography], Marcel Dekker Inc, NY, 2002
[8] Gross, H., editor, [Handbook of Optical Systems (Volume 2), Physical image Formation], Wiley-VCH, 1. Edition, 661 (2005)
[9] O. J. Lokberg, B. E. Seeberg and K. Vestli, "Microscopic video speckle interferometry", Opt. Las. Eng., 26, 313-330, 1997
[10] A. El-Jarad, G. Gülker, and K. Hinsch, "Microscopic ESPI: Better fringe quality by the Fourier transform method", Speckle Metrology 2003, SPIE Vol.4933, p. 335, 2003